Progress In Electromagnetics Research B, Vol. 102, 151–169, 2023

Generalized Approach to Antenna Reconfigurability by Switching Load Admittances

Serafin B. Fischer-Kennedy* **and Jan Hesselbarth**

Abstract—A general theory of a passive multi-port system is presented, incorporating an arbitrary number of feed and load ports. The result is a nonlinear equation system, in which the solution variables are the load admittances, connected to the load ports. The solution ensures impedance match at all feed ports at one particular frequency. It is also shown how this theory can be applied to adaptive and reconfigurable antennas, by using switches to include or exclude some of the load admittances. If, by open state of a switch, the corresponding load admittance is excluded, then the nonlinear equation system is simplified. In general, one load admittance per feed port is required to obtain complex conjugate impedance match. Then, the admittance has a real and an imaginary part, where the real part relates to a resistor, adding loss to the system. It is shown how loss-less matching can be obtained by using two, purely reactive admittances per feed port.

1. INTRODUCTION

Wireless communication systems are becoming ubiquitous. Operation of their antennas may be impacted by ill-defined or varying electromagnetic environment or by excessive tolerances of system's building blocks. Theoretical considerations on antenna property changes due to varying dielectric in their close vicinity are discussed in [1–6], whereas [7–10] pursue a more practical approach regarding changes of the electromagnetic environment. These investigations show that the alteration of the close-by dielectrics change the input impedance and consequently also the resonant frequency of the antenna. A system comprising an antenna and an electronic circuit will suffer since mismatch between antenna and circuit will grow and vary. This can be called internal effect, while the change of the radiation characteristic is an external effect, which is studied in [11, 12]. Similar problems are discussed in [13]. For example, the read-range of an RFID tag may reduce to almost zero if the tag is placed close to a lossy high-permittivity material [14].

In the present work, an antenna that can compensate the internal effect (impedance mismatch) of the changing environment is called adaptive. Theory and methods presented in the following also apply to deliberate reconfiguration of the antenna. Frequency reconfiguration is a subject of extensive research, reviews are given in [15–20]. Most reconfiguration techniques modify currents on the antenna in order to change the resonant frequency, the radiation pattern, the polarization or a combination of them. The modification is realized by active components (e.g., diodes, varactors, MEMS) or by field-biased materials (e.g., ferrites, BST, graphene). Parts of the radiating structure can be connected or disconnected or their capacitive loading can be varied. A particular implementation of reconfiguration is realized in pixel antennas [21–26]. Here, the radiating structure is formed by many small elements, called pixels, which are connected using RF-switches to their neighbouring elements. Upon the reconfiguration requirements, the states of the switches are found by applying genetic algorithms. Some of these works (namely [22, 23]) are using the internal multi-ports method (IMPM), an approach, which is related to

Received 10 July 2023, Accepted 10 August 2023, Scheduled 23 August 2023
* Corresponding author: Serafin B. Fischer-Kennedy (mail@ihf.uni-stuttgart.de).
The authors are with the Institute of Radio Frequency Technology, University of Stuttgart, Germany.

the presented work. In IMPM there are external and internal ports. The external ports allow power flow across the boundaries of the network, whereas internal ports are those with connecting switches. The relationship between all ports is represented by the impedance matrix that, advantageously, must be determined only once. Conditions (e.g., polarization or impedance matching) at the external ports can be enforced, which are then realized by the states of the switches at the internal ports. In the theory part of the present work, load impedances (or load admittances) instead of switch states at the internal ports are determined to fulfill the conditions (here: complex conjugate impedance matching) at the external ports. It turns out that these impedance values can be found as a solution from a nonlinear equation system, which is derived in this work. Further, when using a switch in series with a load impedance, some of these impedances can be activated or deactivated, enabling reconfiguration. Thus, to fulfill the condition at one external port only one switch and one impedance is required.

Another method to compensate environmental effects uses an active-tuned matching network [27–31]. Here, the reflection coefficient at the input of the matching network is observed all the time using, e.g., a directional coupler. If the reflection coefficient becomes worse, the matching network will be tuned accordingly to ensure that most of the power is transferred.

There are also passive means in antenna design to enhance robustness against a changing electromagnetic environment. An intuitive approach is to use a ground plane, that isolates the antenna from the material in the vicinity [32]. Also, well-defined dielectrics as a spacer can be used [33, 34]. For only slight environment alterations, a broad-band antenna as in [35] may be sufficient since the resonant frequency deviates within the frequency bandwidth. A particular concept is presented in [36], where only those characteristic modes of a metal rim cellphone antenna are used that are not severely affected by the user's hand. A passive, suitable power divider network is connected to a dual-fed antenna in [37], realizing matching for two largely different scenarios.

A possible implementation of the concepts derived in this paper is depicted in Fig. 1. A microstrip patch antenna (e.g., of an RFID tag) is able to switch its resonance frequency and can adapt against several, different electromagnetic environments, such as close-by dielectric of varying permittivity. The patch is connected to a chip on the board backside by six transmission lines, two serving as optional (switched) feed points and four serving as (switched) reactive load accesses. Based on the electromagnetic simulation of the antenna including the transmission lines (and considering the electromagnetic environment), the methods described below allow to calculate the required reactive loads.

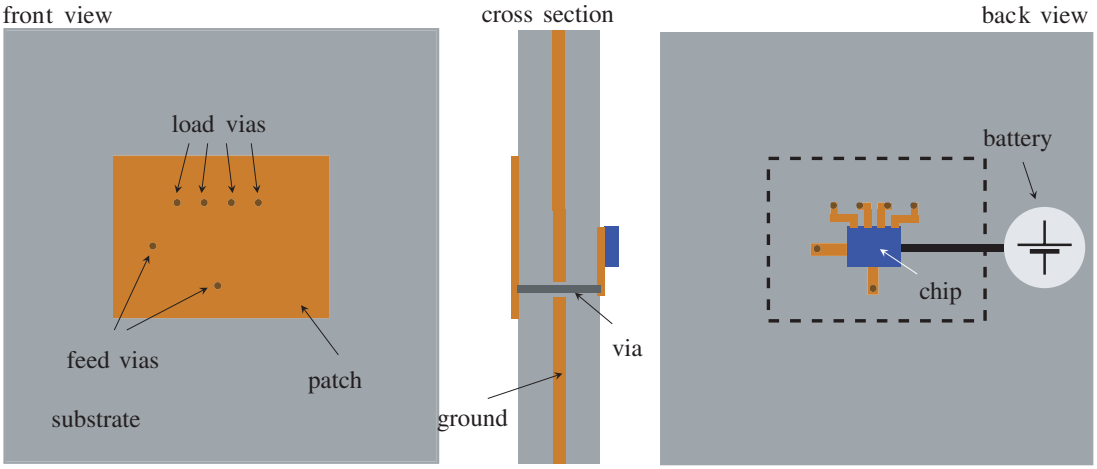

Figure 1. A possible application of the proposed method. A patch antenna, which is doubly fed and loaded with admittances that can be switched to reconfigure the resonance frequency. The chip provides both feeding and switching functions.

This paper is organized as follows. The second section derives a nonlinear equation system, which allows to determine required load admittances. The third section covers three example cases. Firstly, a doubly and simultaneously fed square patch with four load admittances is considered. Secondly, a

rectangular patch study is presented, in which the load impedance distribution over the whole patch is calculated. The third is a frequency-reconfigurable rectangular patch antenna, loaded by switched admittances. The paper ends with a conclusion.

All electromagnetic field simulations used the finite-element solver of CST Microwave Studio software. Calculations were done in Matlab.

2. THEORY

The basic structure of the reconfigurable antenna circuit is separated, as shown in Fig. 2, in an electromagnetic multi-port (EMMP) and a circuit part comprising sources and switched loads. The EMMP is assumed to be known (in this work it is found from an electromagnetic field solver) and is represented by multi-port parameters such as admittance or scattering parameters. The $\mathrm{N}+\mathrm{M}$ ports are grouped into M sources and N loads (Fig. 2). The behavior of the entire structure depends on the states of the switches. Referring to the RFID tag example of Fig. 1, the EMMP comprises patch antenna, vias, lines, while the chip contains the loads, switches, and sources. In this case the EMMP has six ports: two source ports and four load ports.

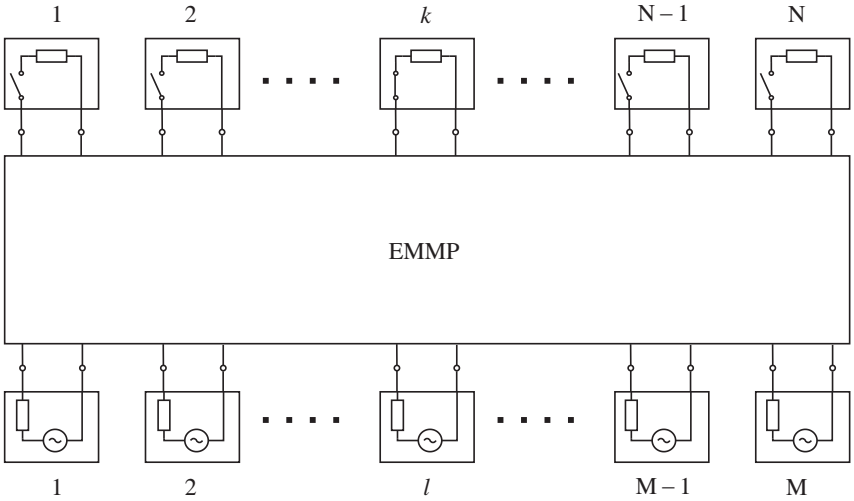

Figure 2. The principal structure of the considered antenna circuit comprising an electromagnetic multi-port (EMMP), N load ports with load admittance and switches, and M source ports with source admittances.

The main goal of the proposed concept is to obtain complex conjugate impedance matching at all source ports at one particular frequency, for one set of settings of the switches. Then, for a different frequency, or, a different electromagnetic environment, the EMMP changes, and matching at all source ports shall be achieved with a different setting of the switches, but with load and source admittances remaining unchanged. Therefore, for a given EMMP, the load admittances are the unknown parameters to be determined. In the derivation of the theory, first, all switches are closed such that all load admittances are contributing to the behavior at the source ports. Later on, the theory is considered with different settings of the switches. The EMMP is supposedly known and represented by

$$\mathbf{Y} = \begin{bmatrix} \mathbf{Y_{ll}} & \mathbf{Y_{ls}} \\ \mathbf{Y_{sl}} & \mathbf{Y_{ss}} \end{bmatrix}, \tag{1}$$

where $\mathbf{Y}$ is a square matrix with complex entries of size $(\mathrm{M}+\mathrm{N}) \times (\mathrm{M}+\mathrm{N})$. This matrix is divided in four sub-matrices: $\mathbf{Y_{ll}} \in \mathbb{C}^{\mathrm{N}\times\mathrm{N}}$, $\mathbf{Y_{ls}} \in \mathbb{C}^{\mathrm{N}\times\mathrm{M}}$, $\mathbf{Y_{sl}} \in \mathbb{C}^{\mathrm{M}\times\mathrm{N}}$ and $\mathbf{Y_{ss}} \in \mathbb{C}^{\mathrm{M}\times\mathrm{M}}$. The index "$\mathbf{l}$" stands for load and "$\mathbf{s}$" for source. Therefore, $\mathbf{Y_{ll}}$ describes the relations between the individual load ports through the EMMP. The sub-matrix $\mathbf{Y_{ls}}$ and $\mathbf{Y_{sl}}$ describe the relations between the source and load ports. "$\mathbf{Y_{ss}}$" gives the relations between all source ports. Further, a load admittance matrix is defined

as

$$\mathbf{Y_L} = \mathrm{diag}(Y_{L_1}, Y_{L_2}, \ldots, Y_{L_k}, \ldots, Y_{L_N}), \tag{2}$$

where Y_{L_k} is the load admittance at the k-th load port. At the source port a source port matrix is defined that represents the known source admittances

$$\mathbf{Y_S} = \mathrm{diag}\,(\mathrm{Y_{S_1}}, \mathrm{Y_{S_2}}, \ldots, \mathrm{Y_{S_l}}, \ldots, \mathrm{Y_{S_M}}). \tag{3}$$

$\mathrm{Y_{S_l}}$ is the source admittance at the l-th source port. The following conversions are performed in order to find a form, which separates the unknown load admittances. According to the definition of the admittance parameters, the currents into all load ports are calculated as

$$\vec{\mathrm{I}}_\mathrm{l} = \mathbf{Y_{ll}}\vec{\mathrm{V}}_\mathrm{l} + \mathbf{Y_{ls}}\vec{\mathrm{V}}_\mathrm{s} \tag{4}$$

and the currents into all source ports as

$$\vec{\mathrm{I}}_\mathrm{s} = \mathbf{Y_{sl}}\vec{\mathrm{V}}_\mathrm{l} + \mathbf{Y_{ss}}\vec{\mathrm{V}}_\mathrm{s}. \tag{5}$$

$\vec{\mathrm{I}}_\mathrm{l}$ and $\vec{\mathrm{V}}_\mathrm{l}$ are vectors whose k-th entry gives the current and voltage of the k-th load port. $\vec{\mathrm{I}}_\mathrm{s}$ and $\vec{\mathrm{V}}_\mathrm{s}$ are vectors whose entries are the currents and voltages of the source ports. The load port currents and voltages relate by the load admittances

$$\vec{\mathrm{I}}_\mathrm{l} = -\mathbf{Y_L}\vec{\mathrm{V}}_\mathrm{l}. \tag{6}$$

The minus sign origins from the definition of port currents, which are always pointing towards the ports. Inserting (6) into (4) and solving for $\vec{\mathrm{V}}_\mathrm{l}$ leads to

$$\vec{\mathrm{V}}_\mathrm{l} = -\left(\mathbf{Y_{ll}} + \mathbf{Y_L}\right)^{-1}\mathbf{Y_{ls}}\vec{\mathrm{V}}_\mathrm{s}. \tag{7}$$

$\left(\mathbf{Y_{ll}} + \mathbf{Y_L}\right)^{-1}$ denotes the inverse matrix of matrix $\left(\mathbf{Y_{ll}} + \mathbf{Y_L}\right)$. By inserting (7) into (5), the following relation for the current at the source ports is obtained

$$\vec{\mathrm{I}}_\mathrm{s} = \left(\mathbf{Y_{ss}} - \mathbf{Y_{sl}}\left(\mathbf{Y_{ll}} + \mathbf{Y_L}\right)^{-1}\mathbf{Y_{ls}}\right)\vec{\mathrm{V}}_\mathrm{s}. \tag{8}$$

Considering the source port as it is shown exemplary for the l-th source port in Fig. 3, the following relation holds

$$\vec{\mathrm{I}}_\mathrm{s} = \mathbf{Y_S}\vec{\mathrm{V}}_0 - \mathbf{Y_S}\vec{\mathrm{V}}_\mathrm{s}. \tag{9}$$

Here, $\vec{\mathrm{V}}_0$ is a vector including all source voltages at the respective source ports. Furthermore, a voltage divider between the source and the source port voltage is applied and expressed with matrices at all source ports

$$\vec{\mathrm{V}}_\mathrm{s} = \left(\mathbf{Y_S} + \mathbf{Y_{in}}\right)^{-1}\mathbf{Y_S}\vec{\mathrm{V}}_0 = \mathbf{M_{vr}}\vec{\mathrm{V}}_0. \tag{10}$$

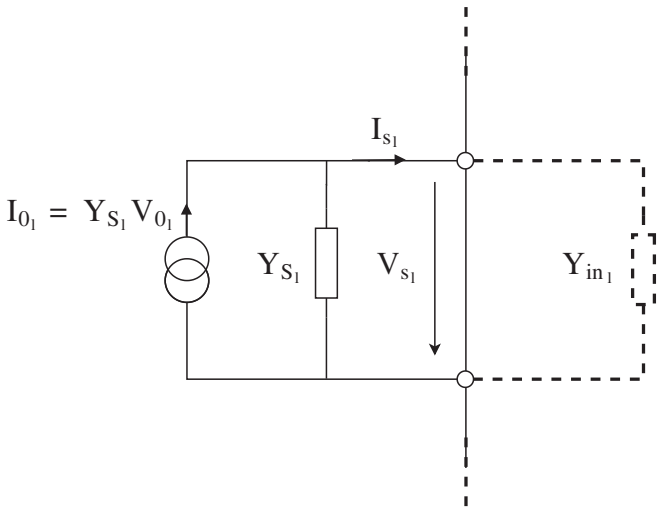

Figure 3. Current, voltage and admittance labeling at the l-th source port.

Here,

$$\mathbf{Y_{in}} = \mathrm{diag}\left(\mathrm{Y_{in_1}}, \mathrm{Y_{in_2}}, \ldots, \mathrm{Y_{in_l}}, \ldots, \mathrm{Y_{in_M}}\right) \tag{11}$$

is a diagonal matrix with the input admittances (active admittances) at the respective source port, and $\mathbf{M_{vr}}$ is a diagonal matrix named voltage ratio matrix. Mutual substitution of (8)–(10) results in

$$\mathbf{Y_s}(\mathbf{I_M}-\mathbf{M_{vr}})\vec{\mathrm{V}}_0 = \left(\mathbf{Y_{ss}} - \mathbf{Y_{sl}}\left(\mathbf{Y_{ll}}+\mathbf{Y_L}\right)^{-1}\mathbf{Y_{ls}}\right)\mathbf{M_{vr}}\vec{\mathrm{V}}_0 \tag{12}$$

with the identity matrix $\mathbf{I_M}$ of size M. The matching condition at the source ports is

$$\mathbf{Y_{in}} = \overline{\mathbf{Y_S}} = \mathrm{diag}\left(\mathrm{Y}^*_{\mathrm{S_1}}, \mathrm{Y}^*_{\mathrm{S_2}}, \ldots, \mathrm{Y}^*_{\mathrm{S_l}}, \ldots, \mathrm{Y}^*_{\mathrm{S_M}}\right). \tag{13}$$

Here, $\overline{\mathbf{Y_S}}$ denotes the complex conjugate matrix of $\mathbf{Y_S}$ and $\mathrm{Y}^*_{\mathrm{S_l}}$ the complex conjugate of $\mathrm{Y_{S_l}}$. In (12), $\mathbf{M_{vr}}$ is the only matrix, that is dependent on $\mathbf{Y_{in}}$, therefore

$$\mathbf{M_{vr}} = \left(\mathbf{Y_S} + \overline{\mathbf{Y_S}}\right)^{-1}\mathbf{Y_S} = \frac{1}{2}\,\mathrm{Re}\{\mathbf{Y_S}\}^{-1}\mathbf{Y_S} = \frac{1}{2}\left(\mathbf{I_M} + \mathrm{j}\,\mathrm{Re}\{\mathbf{Y_S}\}^{-1}\,\mathrm{Im}\{\mathbf{Y_S}\}\right) \tag{14}$$

and $\mathbf{I_M}-\mathbf{M_{vr}} = 1/2\left(\mathbf{I_M} - \mathrm{j}\,\mathrm{Re}\{\mathbf{Y_S}\}^{-1}\,\mathrm{Im}\{\mathbf{Y_S}\}\right)$ with j as the imaginary unit. If the source admittances have only a real part, the voltage ratio matrix becomes the identity matrix multiplied by 1/2. With the relation $\mathbf{A^{-1}} = \mathrm{adj}\left(\mathbf{A}\right)/\det\left(\mathbf{A}\right)$ for an invertible square matrix $\mathbf{A}$ the expression of (12) changes to

$$\det\left(\mathbf{Y_{ll}}+\mathbf{Y_L}\right)\mathbf{Y_s}\left(\mathbf{I_M}-\mathbf{M_{vr}}\right)\vec{\mathrm{V}}_0 = \det\left(\mathbf{Y_{ll}}+\mathbf{Y_L}\right)\mathbf{Y_{ss}}\mathbf{M_{vr}}\vec{\mathrm{V}}_0 - \mathbf{Y_{sl}}\,\mathrm{adj}\left(\mathbf{Y_{ll}}+\mathbf{Y_L}\right)\mathbf{Y_{ls}}\mathbf{M_{vr}}\vec{\mathrm{V}}_0. \tag{15}$$

Thereby, $\mathrm{adj}\left(\mathbf{A}\right)$ indicates the adjugate matrix of $\mathbf{A}$. Still, the goal is to separate the knowns from the unknowns; therefore, the following relations (from section 5 of [38]) are applied

$$\det(\mathbf{Y_{ll}}+\mathbf{Y_L}) = \sum_{j=0}^{2^{\mathrm{N}}-1}\det\left(\mathbf{P^T_{S(j)}}\mathbf{Y_{ll}}\mathbf{P_{S(j)}}\right)\prod_{i\in\mathrm{S(j)}}Y_{L_i} \tag{16}$$

$$\mathrm{adj}(\mathbf{Y_{ll}}+\mathbf{Y_L}) = \sum_{j=0}^{2^{\mathrm{N}}-1}\mathbf{P_{S(j)}}\,\mathrm{adj}\left(\mathbf{P^T_{S(j)}}\mathbf{Y_{ll}}\mathbf{P_{S(j)}}\right)\mathbf{P^T_{S(j)}}\prod_{i\in\mathrm{S(j)}}Y_{L_i} \tag{17}$$

where S is a index set of all possible combinations out of $\{1,\ldots,\mathrm{N}\}$ without repetition in a lexicographical order. For example, if $\mathrm{N}=3$, then

$$\mathrm{S} := \{\{\},\{1\},\{2\},\{3\},\{1,2\},\{1,3\},\{2,3\},\{1,2,3\}\}$$

with entry $\mathrm{S}(0) = \varnothing$ (the empty element) and entry $\mathrm{S}(4) = \{1,2\}$. Further, $\mathbf{P_{S(j)}}$ denotes the identity matrix of size N, in which the columns, indexed by the set S(j), are removed. Inserting this relation into (15) results in

$$\sum_{j=1}^{2^{\mathrm{N}}-1}\vec{\mathrm{k_j}}\prod_{i\in\mathrm{S(j)}}Y_{L_i} = \vec{\mathrm{r}} \tag{18}$$

with

$$\vec{\mathrm{k_j}} = \left(\left(\mathbf{Y_{ss}}+\mathbf{Y_S}\right)\mathbf{M_{vr}} - \mathbf{Y_S}\right)\det\left(\mathbf{P^T_{S(j)}}\mathbf{Y_{ll}}\mathbf{P_{S(j)}}\right)\vec{\mathrm{V}}_0 - \mathbf{Y_{sl}}\mathbf{P_{S(j)}}\,\mathrm{adj}\left(\mathbf{P^T_{S(j)}}\mathbf{Y_{ll}}\mathbf{P_{S(j)}}\right)\mathbf{P^T_{S(j)}}\mathbf{Y_{ls}}\mathbf{M_{vr}}\vec{\mathrm{V}}_0$$

and

$$\vec{\mathrm{r}} = \det(\mathbf{Y_{ll}})(\mathbf{Y_S} - (\mathbf{Y_{ss}}+\mathbf{Y_S})\mathbf{M_{vr}})\vec{\mathrm{V}}_0 + \mathbf{Y_{sl}}\,\mathrm{adj}\left(\mathbf{Y_{ll}}\right)\mathbf{Y_{ls}}\mathbf{M_{vr}}\vec{\mathrm{V}}_0.$$

Equation (18) can be expressed in matrix form to

$$\mathbf{K}\vec{v_l} = \vec{\mathrm{r}} \tag{19}$$

with matrix

$$\mathbf{K} = \left(\vec{\mathrm{k}}_1, \ldots, \vec{\mathrm{k_j}}, \ldots \tilde{\mathrm{k}}_{(2^{\mathrm{N}}-1)}\right)$$

and the load vector

$$\vec{v_l} = \left(Y_{L_1}, \ldots, Y_{L_N}, Y_{L_1}Y_{L_2}, \ldots, Y_{L_{N-1}}Y_{L_N}, \ldots, \ldots, Y_{L_1}Y_{L_2}\cdots Y_{L_{N-1}}Y_{L_N}\right)^{\mathrm{T}}$$

where the entries are the lexicographical ordered combinations out of all load admittances without repetitions. Here, $\mathbf{K} \in \mathbb{C}^{\mathrm{M}\times 2^{\mathrm{N}}-1}$, $\vec{v_l} \in \mathbb{C}^{2^{\mathrm{N}}-1\times 1}$ and $\vec{\mathrm{r}} \in \mathbb{C}^{\mathrm{M}\times 1}$. Equation (19) is a nonlinear equation system. $\vec{v_l}$ is to be found, such that (19) is fulfilled, thereby matching all source ports for the considered case.

2.1. Switching the Load Admittances

Based on the theory for an EMMP with loads and sources derived so far, the example of Fig. 1 above will illustrate the concept. The principal structure with two sources (M = 2) and four switched load admittances (N = 4) is shown in Fig. 4. If all switches are closed, (19) has the following form:

$$\begin{bmatrix} \mathrm{k}_{11} & \mathrm{k}_{12} & \cdots & \mathrm{k}_{1(15)} \\ \mathrm{k}_{21} & \mathrm{k}_{22} & \cdots & \mathrm{k}_{2(15)} \end{bmatrix} \begin{pmatrix} Y_{L_1} \\ Y_{L_2} \\ Y_{L_3} \\ Y_{L_4} \\ Y_{L_1}Y_{L_2} \\ Y_{L_1}Y_{L_3} \\ Y_{L_1}Y_{L_4} \\ Y_{L_2}Y_{L_3} \\ Y_{L_2}Y_{L_4} \\ Y_{L_3}Y_{L_4} \\ Y_{L_1}Y_{L_2}Y_{L_3} \\ Y_{L_1}Y_{L_2}Y_{L_4} \\ Y_{L_1}Y_{L_3}Y_{L_4} \\ Y_{L_2}Y_{L_3}Y_{L_4} \\ Y_{L_1}Y_{L_2}Y_{L_3}Y_{L_4} \end{pmatrix} = \begin{pmatrix} \mathrm{r}_1 \\ \mathrm{r}_2 \end{pmatrix} \tag{20}$$

The equation system (20) is underdetermined, with 4 unknowns and two equations. Therefore, the switches of load admittances Y_{L_3} and Y_{L_4} are put "open" reducing the number of unknowns to two, since $Y_{L_3} = Y_{L_4} = 0$. Equation (20) is simplified then to

$$\begin{bmatrix} \mathrm{k}_{11} & \mathrm{k}_{12} & \mathrm{k}_{15} \\ \mathrm{k}_{21} & \mathrm{k}_{22} & \mathrm{k}_{25} \end{bmatrix} \begin{pmatrix} Y_{L_1} \\ Y_{L_2} \\ Y_{L_1}Y_{L_2} \end{pmatrix} = \begin{pmatrix} \mathrm{r}_1 \\ \mathrm{r}_2 \end{pmatrix}, \tag{21}$$

and a solution can be found. A change of the frequency or of the environment of the antenna will alter the EMMP, i.e., the matrix $\mathbf{K}$ and vector $\vec{\mathrm{r}}$, but the source shall remain matched. Then, the switches of load admittances Y_{L_3} and Y_{L_4} are closed and Y_{L_1} and Y_{L_2} are opened. Consequently, $Y_{L_1} = Y_{L_2} = 0$

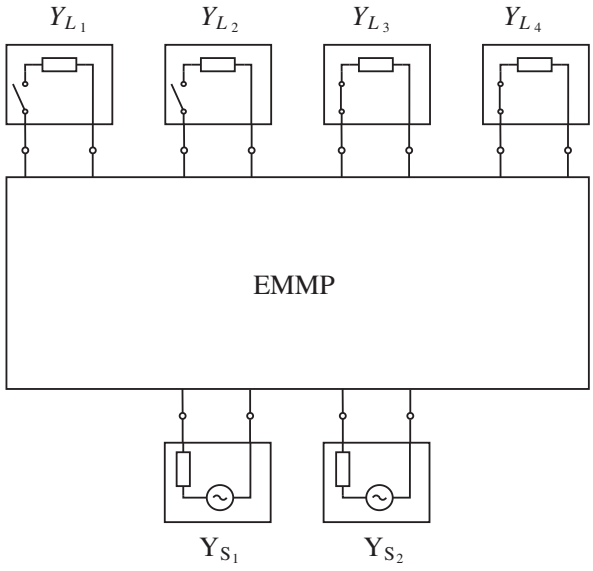

Figure 4. The principle structure of the considered example with N = 4 load admittances and M = 2 sources.

and

$$\begin{bmatrix} \mathrm{k}'_{13} & \mathrm{k}'_{14} & \mathrm{k}'_{1(10)} \\ \mathrm{k}'_{23} & \mathrm{k}'_{24} & \mathrm{k}'_{2(10)} \end{bmatrix} \begin{pmatrix} Y_{L_3} \\ Y_{L_4} \\ Y_{L_3} Y_{L_4} \end{pmatrix} = \begin{pmatrix} \mathrm{r}'_1 \\ \mathrm{r}'_2 \end{pmatrix}. \tag{22}$$

The prime of matrix $\mathbf{K}$ and vector $\vec{\mathrm{r}}$ indicate the change of the EMMP. Note that for non-perfect, but known, switches (e.g., $Y_{L_1} = Y_{L_2} \neq 0$) the equation system can be rearranged to obtain the same form as in (21) and (22).

3. EXAMPLES

The first example verifies the general theory, therefore, two feed ports and four load ports are used. Further, in the second example, a rectangular patch antenna with only one feed and load port is considered. This example shows, how the load admittance behaves when changing the load location. In the last example, a possibility is shown to apply the concept to frequency reconfiguration.

3.1. A Doubly and Simultaneously Fed Square Patch

The first example shows how the theory can be used in antenna design. The object of the investigation is exclusively the calculation of the load admittances of a doubly edge-fed square patch antenna without considering the switching option. In Fig. 5 the structure is depicted. The square patch antenna ($70 \times 70\,\mathrm{mm}^2$) is modeled on a 2 mm-thick FR4 substrate with a relative permittivity of 4.3 and a ground plane on its backside. 50 Ω-feed lines, that have a width of 3.75 mm are placed orthogonal to each other extending from the edges of the square patch to the ends of the substrate. In order to incorporate the loads, load structures using vias with a radius of 0.3 mm are implemented as shown in Fig. 6(a) for one exemplary load. From the patch (orange colored), a via is connected to a small circular disc (with a radius of 0.6 mm) on the bottom, which is then connected over a surface-mounted device (SMD), e.g., a capacitor or inductor to the ground plane. The circular gap is 1 mm, and the gap for the SMD has a width of 0.6 mm.

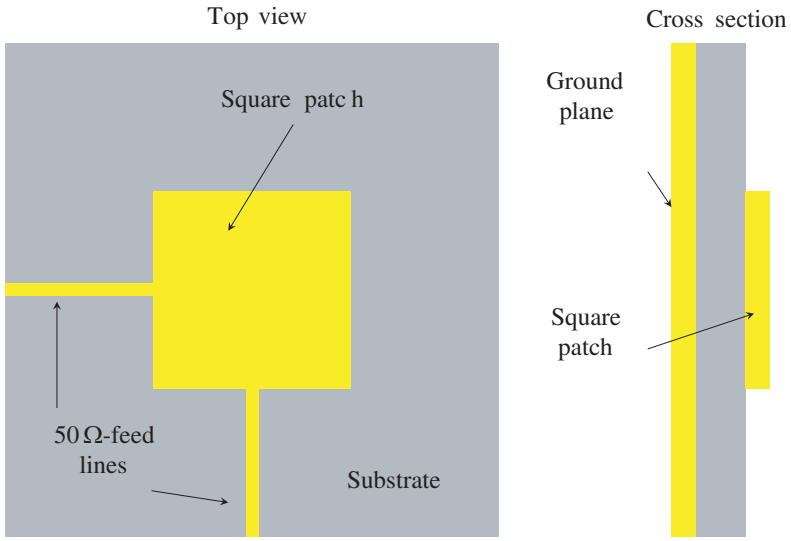

Figure 5. The structure of a doubly edge-fed square patch.

Since the edge impedance of the patch is different in comparison to the source impedance, which is 50 Ω at the considered frequency of 1 GHz, there is no inherent impedance matching. It is also clear that if the two sources are matched, their powers are combined within the square patch. To avoid losses in

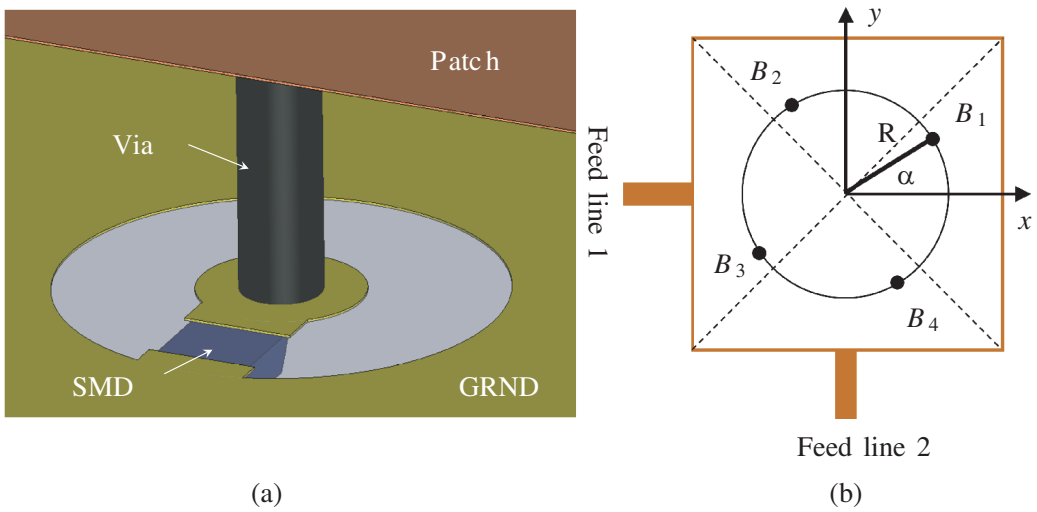

Figure 6. Insertion of load susceptances in the patch antenna circuit of Fig. 5. (a) via with surface-mount (SMD) shunt susceptance on the board backside (dielectric set transparent); (b) symmetrical positions of four shunt susceptances (denoted B_1, B_2, B_3, B_4) at positions, which are defined by parameters R and α.

the load admittances the real parts are set to zero. Then (19) can be rewritten in a purely real equation system

$$\mathrm{Re}\{\mathbf{K}\}\,\mathrm{Re}\{\vec{v_l}\} - \mathrm{Im}\{\mathbf{K}\}\,\mathrm{Im}\{\vec{v_l}\} = \mathrm{Re}\{\vec{\mathrm{r}}\} \tag{23a}$$

$$\mathrm{Re}\{\mathbf{K}\}\,\mathrm{Im}\{\vec{v_l}\} + \mathrm{Im}\{\mathbf{K}\}\,\mathrm{Re}\{\vec{v_l}\} = \mathrm{Im}\{\vec{\mathrm{r}}\} \tag{23b}$$

This has doubled the number of equations. In this example, for lossless matching, there are four equations, for which four load susceptances are required. This leads to a $\mathbf{K}$ matrix of size (2×15) and a $\vec{\mathrm{r}}$ vector of size (2×1). The question is where these loads should be inserted. Since the positions of the load ports represent many degrees of freedom, it is interesting to investigate how the load suceptances behave by varying these locations. Therefore, the loads positions are arbitrarily parameterized in polar coordinates according to Fig. 6(b) to

$$\mathrm{x_{i+1}} = \mathrm{R}\cos\left(\alpha + \mathrm{i}\frac{\pi}{2}\right) \tag{24a}$$

$$\mathrm{y_{i+1}} = \mathrm{R}\sin\left(\alpha + \mathrm{i}\frac{\pi}{2}\right), \tag{24b}$$

where $\mathrm{i} = 0, 1, 2, 3$. At the position $(\mathrm{x_{i+1}}, \mathrm{y_{i+1}})$ the susceptance B_{i+1} with $Y_{L_{1+i}} = \mathrm{j}B_{i+1}$ is inserted. Following steps are performed to find all the loads:

- Modelling of the antenna including the feed and load structure.
- S-parameters simulation at 1 GHz in *CST Microwave Studio* of the design, all feeds and loads are represented by ports (six in total).
- Export of the six port S-parameters from *CST* and import in *MATLAB*.
- Calculating the load susceptances:
  1. S to Y parameters conversion.
  2. Calculation of $\mathbf{K}$ matrix and vector $\vec{\mathrm{r}}$ after (18).
  3. Setting up nonlinear equation system as in (19).
  4. Solving it numerically.

These steps are done for varying values of R and α, and the susceptances are calculated at 1 GHz. In Fig. 7, the calculated load susceptances for various angles (a)–(d) over the radius R and various radii (e)–(f) over angle α are depicted. It should be noted that not for every position an exact solution is found.

Some points show an error, which is in the worst case still less than 10^{-7} with error $= \max(|\mathbf{K}\vec{v}_l - \vec{r}|)$). It is by no means clear that a solution can be found for every arbitrary EMMP. On the other hand, there can also be multiple solutions. Considering now the graphs (a) to (d) of Fig. 7. In all the values of these graphs, the mirror image to the diagonal from the lower left to the upper right corner of the structure as in Fig. 6(c) is reflected. In (a), where $\alpha = 0°$, the values of B_1 are equal to the ones of B_2. Also the values of B_3 are equal to the values of B_4. Sub figure (d) can be obtained from (b) by interchange B_2 and B_4. Susceptances B_1 and B_3 remain untouched. This comes from the fact that, if the structure of $\alpha = 22.5°$ is mirrored along the diagonal from the lower left to the upper right corner, the structure of $\alpha = 67.5°$ is replicated. For $\alpha = 45°$, which is (c), B_1 and B_3 are located on the diagonal. The behavior of this two values over R deviates but shows a similar course. In Fig. 7(e) the susceptances over the angle α for the radius R = 5 mm and in (f) for R = 30 mm are depicted.

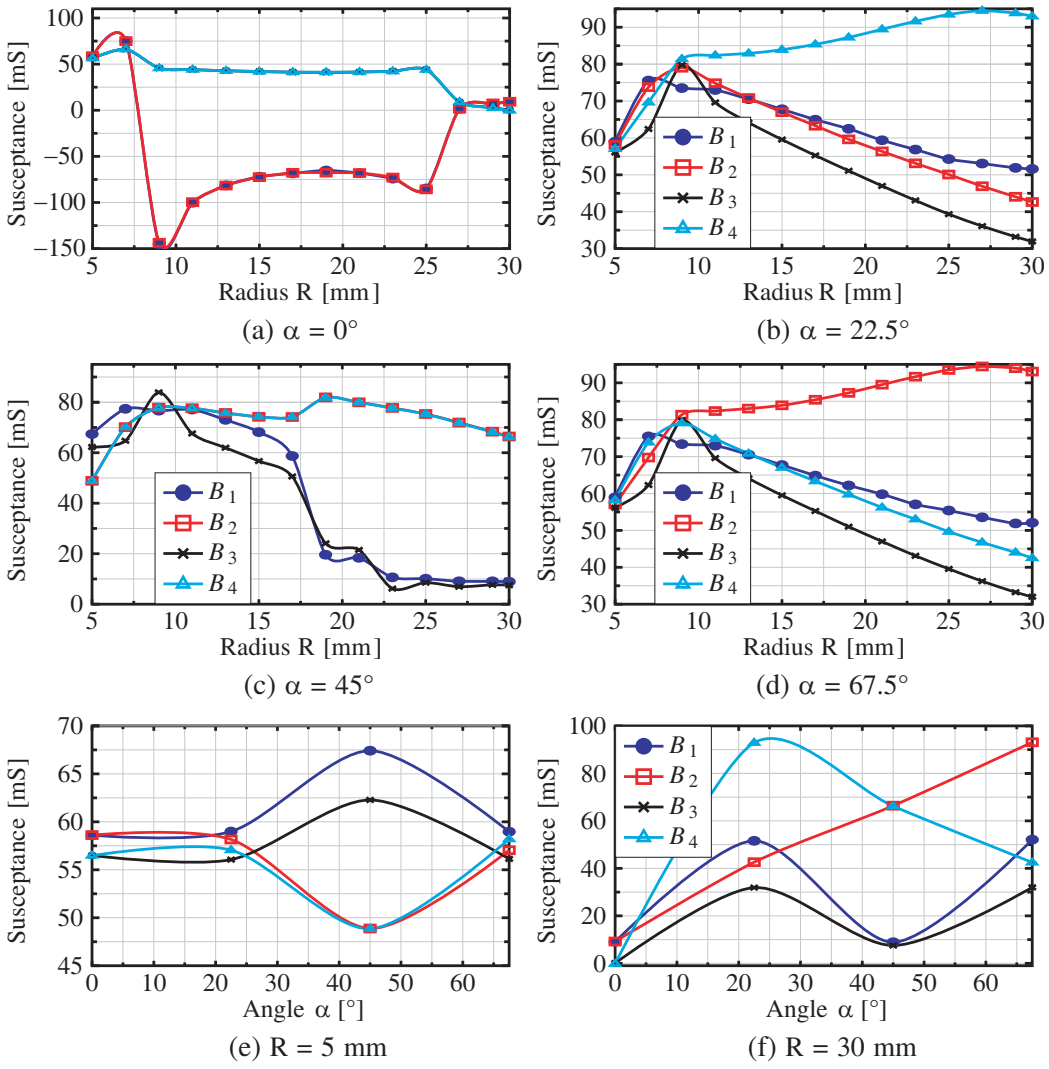

Figure 7. The calculated load susceptances at 1 GHz for various angle (a)–(d) over the radius R and various radii (e)–(f) over angle α. All legends are the same and shown on top of the two first graphs.

In addition, the frequency behaviors of the load susceptances with $\alpha = 45°$ are shown in Fig. 8 for different radii of R. The behaviors of B_1 and B_3 as well as B_2 and B_4 are approximately the same (cf. Fig. 7), which is the reason that B_1 and B_2 are shown only. The curves of all susceptances for R = 5 mm and 17 mm show points of discontinuities.

The input impedance Z_{in_1} at source port one and Z_{in_2} at source port two, when the EMMP is loaded

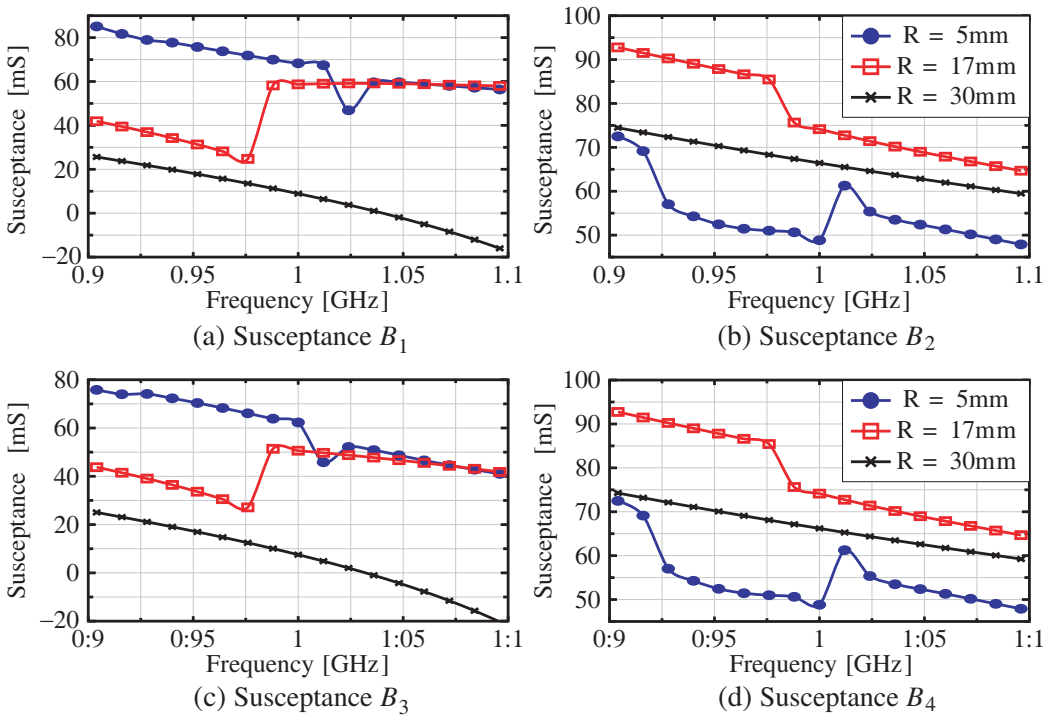

Figure 8. The four susceptances over the frequency for three different values of R with $\alpha = 45°$. The legends of all graphs are same as in (b) and (d).

with the calculated respective susceptances, are depicted in Fig. 9. The behaviors of the resistance (a) and reactance (b) of the input impedances over the frequency for three different values of the radius R (5 mm, 17 mm and 30 mm and for $\alpha = 45°$ are shown. Thereby, the sources are simultaneously exciting the EMMP. Here again, the structures' symmetry is reflected in the values of Z_{in_1} and Z_{in_2}, which are the same. In the plots, there are two orthogonal dashed lines shown. At the locations, where these lines are crossing each other, the EMMP with the respective loads are fulfilling (19). At these locations, the variation of the impedances over frequency deviates, even if the variation of the load susceptances over frequency showing similar slopes (cf. Fig. 8).

It is also worth evaluating the solutions in terms of the field parameters, such as the surface current. Therefore, the calculated susceptances (here: capacitors) are included in the field simulation. In Fig. 10 the surface current at 1 GHz on the square patch for (a) R = 5 mm, (b) 17 mm and (c) 30 mm at a value of α of 45° is depicted. Obviously, there is an increased current density around the load locations resulting in a current distribution much different from the case without loads.

3.2. Loaded Patch Study

In this example a single edge-fed rectangular patch antenna is considered as shown in Fig. 11. The patch is fed by a 50 Ω microstrip transmission line (MTL) directly at the edge. A load impedance is inserted in the same way as in the previous example (cf. Figs. 6(a)–(b) with a via radius of 0.3 mm) in order to match the antenna at 1 GHz. Here, the idea is to see the behavior of the load impedance in dependency of the load position over the whole patch. The half-wavelength patch is on a FR4 substrate with a relative permittivity of 4.3 and a height of 2 mm. For dimensions refer to Fig. 11.

For an EMMP with only one source and one load, (19) is simplified and can be solved after the load admittance to

$$Y_L = \frac{r_1}{k_{11}} = \frac{Y_{sl} Y_{ls}}{Y_{ss} - Y_0} - Y_{ll}, \tag{25}$$

with the source admittance of $Y_0 = 20$ mS. The formula shows that, if the patch would be inherently

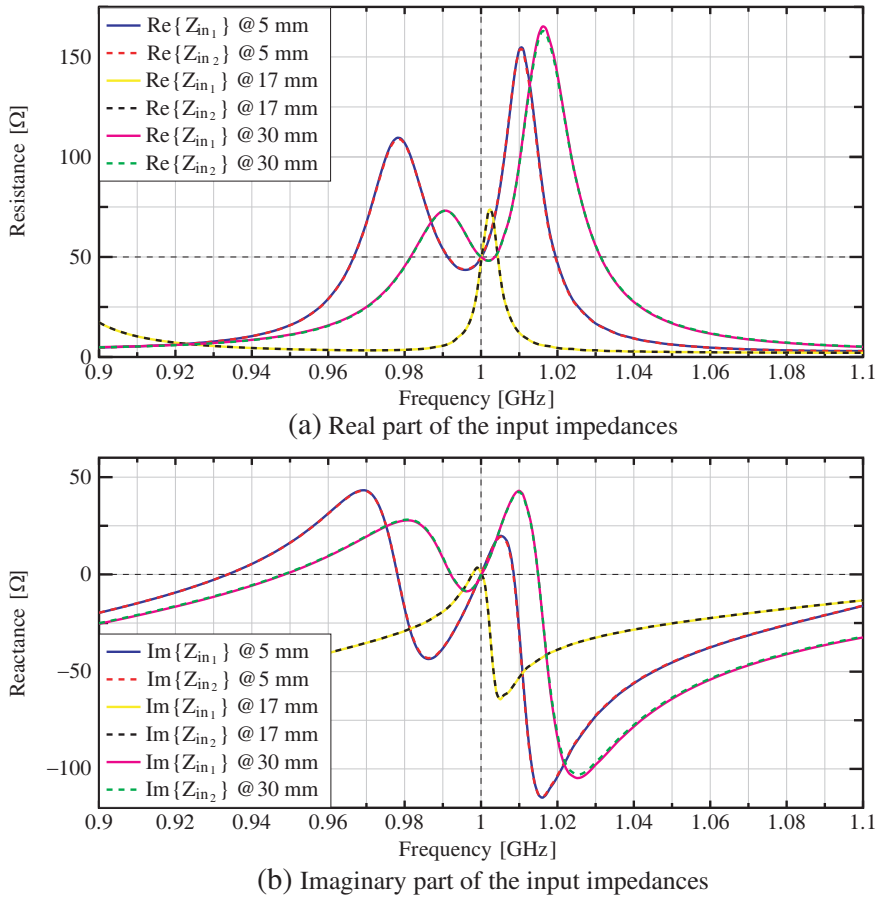

Figure 9. The input impedances Z_{in_1} and Z_{in_2} at both source ports (simultaneous feed) for different values of R over frequency. $Z_{in_1} = Z_{in_2}$ for the special case (shown in Figure) $\alpha = 45°$.

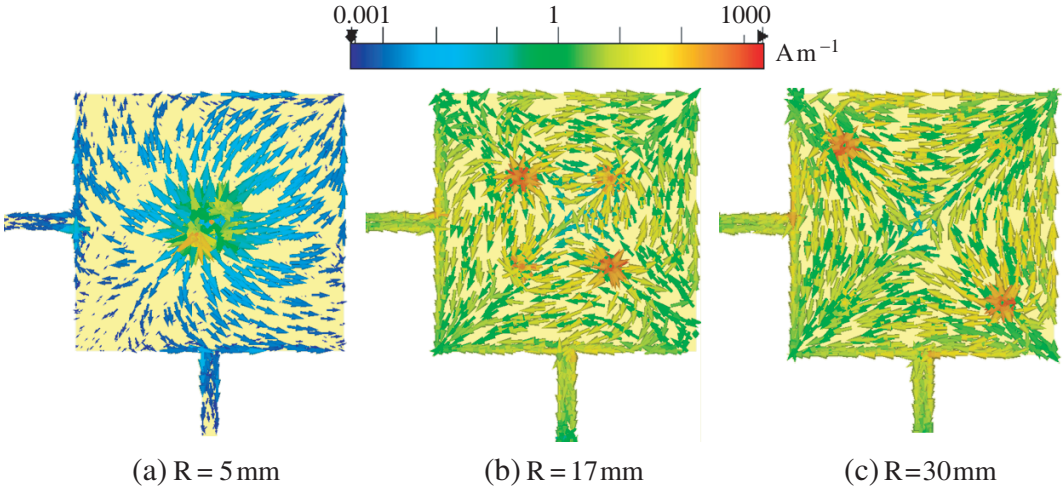

Figure 10. The magnitude of the surface current (logarithmic scale) with simultaneous excitation on the square patch for $\alpha = 45°$ and various radii of R.

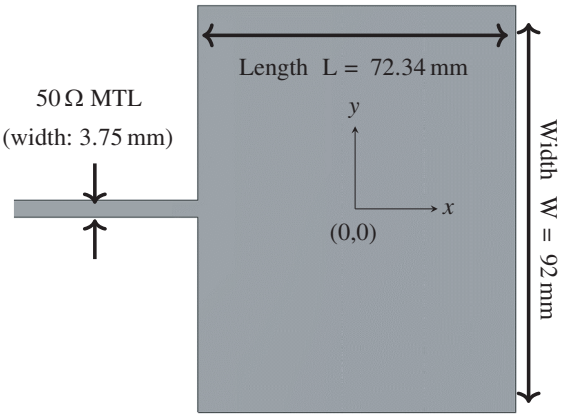

Figure 11. Layout and coordinate system of an edge-fed rectangular patch antenna. All conductors are perfectly electrically conductive and the relative permittivity of the lossless substrate is $\epsilon_r = 4.3$.

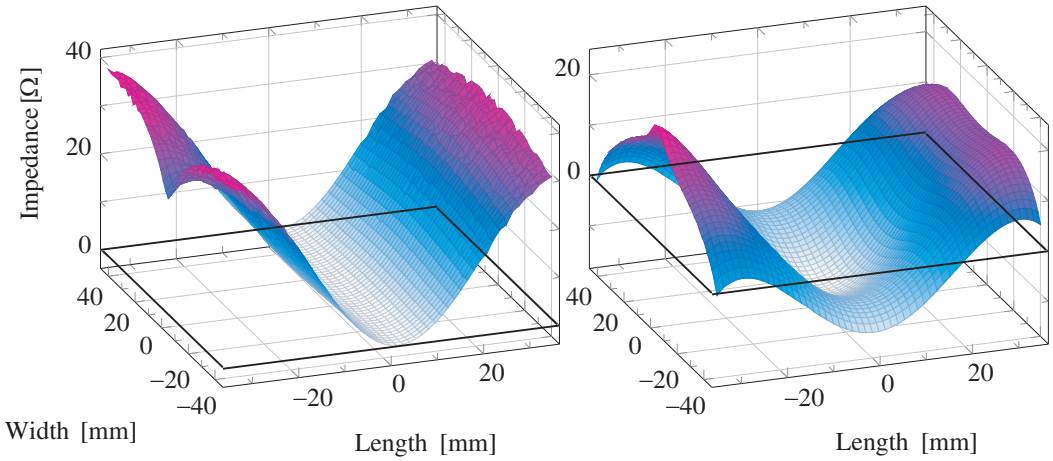

(a) Real part (b) Imaginary part

Figure 12. The real (a) and imaginary (b) part of the load impedance over its position within the rectangular patch.

matched, which means $Y_{ss} = Y_0$ (real values) the load admittance approaches infinity, meaning, a short circuit at the load port. For each point in the xy-plane (see coordinate system in Fig. 11) on the patch, this formula is evaluated, thereby, the symmetry to the xz-plane of the load admittance values is exploited (the whole patch is field simulated). Then, the load impedance is calculated at 1 GHz and the result is plotted in Fig. 12. (a) shows the real and (b) the imaginary part of the load impedance. Additionally, the black lines in the plots are indicating the patch antenna.

Figure 13 is an elevation plot view of Fig. 12(b) with the same color scale. The white lines are indicating at which locations the imaginary part of the load impedance becomes zero (cut with the xy-plane of the plot in Fig. 12(b). At the same time, they mark the transition from one region to the other. Capacitive region means that in this region a capacitor must be used, consequently, in the inductive region a inductor must be taken. The dotted black lines are showing the locations, where the real part of the load impedance becomes zero (cut with the xy-plane of the plot in Fig. 12(a)). Along these lines lossless impedance matching is possible.

In Fig. 14 the surface current on the patch and the radiation characteristic in dBi in the xy-plane

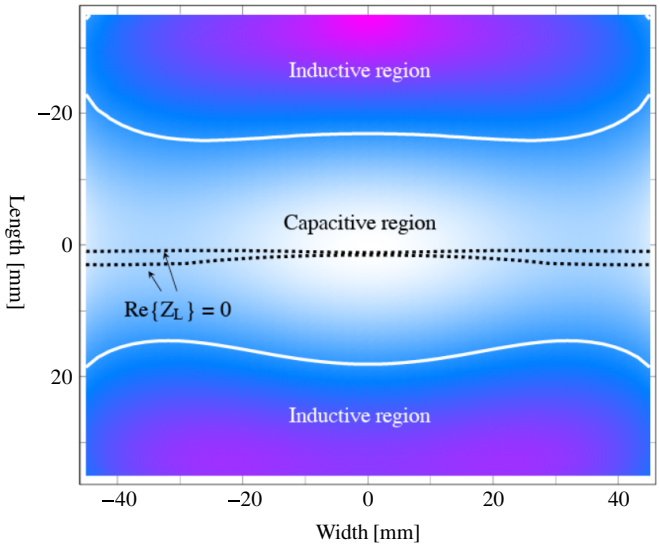

Figure 13. Different regions of the rectangular patch antenna. The white lines are indicating where the imaginary part and the black dotted lines where the real part of the load impedances become zero.

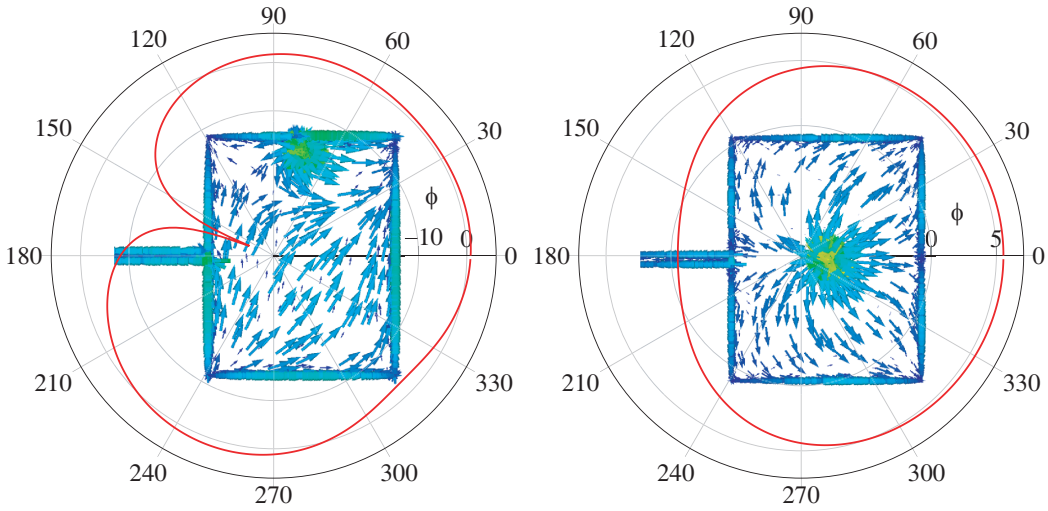

(a) Load location: (x = 0.72 mm, y = 40 mm) (b) Load location: (x = 0.62 mm, y = 0 mm)

Figure 14. The gain in dBi in the xy-plane (red) and xz-plane (blue) of the patch and the corresponding surface current on the patch for two different locations of load impedances.

(red curve) and xz-plane (blue curve) for two different locations is depicted. Both locations are chosen according to the load region plot (Fig. 13), such that the real part of the load impedance is zero. Two very different locations are used, (a) at at the edge and (b) in the middle of the patch. As can be seen, the surface current distribution is much different between these two cases leading also to two different radiation characteristics. The corresponding reflection coefficient over frequency of the case in (b) can be seen in the graph of Fig. 15 (blue curve, labeled with "1"). This curve shows a very narrowband behavior since there are no losses.

In addition, Table 1 lists the load impedances for different positions along the line $y = 0$. The respective reflection coefficients are shown in Fig. 15. The labels in the legend are chosen as it is in the table. The table also reports the radiation efficiency. The degradation of the radiation efficiency is solely because of the resistance in the load impedance. These losses are also reflected in the bandwidth

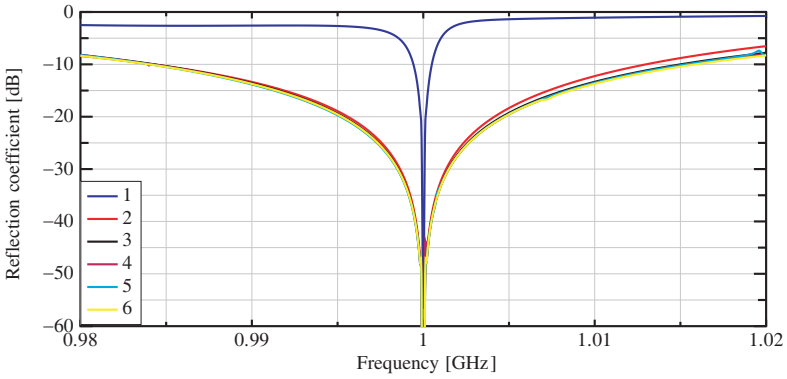

Figure 15. The reflection coefficient in dB over frequency for different locations of the load impedance after Table 1.

Table 1. The calculated load impedances at different locations and the respective efficiencies of the rectangular patch antenna at 1 GHz.

Label	Location (x, y)	Load impedance	Rad. efficiency
1	(0.62 mm, 0 mm)	$-\mathrm{j}14.824\,\Omega$	100%
2	(7 mm, 0 mm)	$(2.154 - \mathrm{j}12.262)\,\Omega$	18%
3	(14 mm, 0 mm)	$(9.67 - \mathrm{j}5.24)\,\Omega$	16%
4	(21 mm, 0 mm)	$(20.865 + \mathrm{j}3.430)\,\Omega$	15.5%
5	(28 mm, 0 mm)	$(30.850 + \mathrm{j}10.643)\,\Omega$	15.2%
6	(35 mm, 0 mm)	$(36.453 + \mathrm{j}12.798)\,\Omega$	14.9%

behavior of the reflection coefficients in Fig. 15, which is much wider than in the case "1" with purely reactive load.

3.3. Frequency Reconfiguration by Load Admittances of a Patch Antenna

In this example an edge-fed rectangular patch antenna after Fig. 11 (the substrate thickness is 2 mm and the relative permittivity is 4.3) is considered. To be able to reconfigure two different resonant frequencies the patch is loaded with four susceptances. Note, that a frequency variation of 6% is much larger than the frequency bandwidth of this very thin patch antenna. The loads are incorporated into the antenna as in the previous examples (cf. Fig. 6 with a via radius of 0.3 mm). A purely lossless matching is aimed, which is the reason why four instead of two loads are required. So, it is an N = 4, M = 1 EMMP. For the first frequency $\mathrm{f}_1 = 0.97\,\mathrm{GHz}$, the susceptances B_{L_1} and B_{L_2} should be active, while the other ones are open circuited ($B_{L_3} = B_{L_4} = 0$). For $\mathrm{f}_2 = 1.03\,\mathrm{GHz}$ it is the other way around, B_{L_1} and B_{L_2} are open circuited. After (19) following equations can be stated:

$$\mathrm{k}_{11}^{\mathrm{f}_1}\mathrm{j}B_{L_1} + \mathrm{k}_{12}^{\mathrm{f}_1}\mathrm{j}B_{L_2} - \mathrm{k}_{15}^{\mathrm{f}_1}B_{L_1}B_{L_2} = \mathrm{r}_1^{\mathrm{f}_1} \tag{26a}$$

$$\mathrm{k}_{13}^{\mathrm{f}_2}\mathrm{j}B_{L_3} + \mathrm{k}_{14}^{\mathrm{f}_2}\mathrm{j}B_{L_4} - \mathrm{k}_{1(10)}^{\mathrm{f}_2}B_{L_3}B_{L_4} = \mathrm{r}_1^{\mathrm{f}_2}. \tag{26b}$$

The superscripts indicate at which frequency (f_1 or f_2) the $\mathbf{K}$ matrix and $\tilde{\mathrm{r}}$ vector are evaluated. Obviously, these equations are independent from each other, and each one is in turn fully determined, when being rewritten in a purely real valued equation system. Then

$$\mathrm{Re}\{\mathrm{r}_1^{\mathrm{f}_1}\} + \mathrm{Im}\{\mathrm{k}_{11}^{\mathrm{f}_1}\}B_{L_1} + \mathrm{Im}\{\mathrm{k}_{12}^{\mathrm{f}_1}\}B_{L_2} + \mathrm{Re}\{\mathrm{k}_{15}^{\mathrm{f}_1}\}B_{L_1}B_{L_2} = 0 \tag{27a}$$

$$\mathrm{Im}\{\mathrm{r}_1^{\mathrm{f}_1}\} - \mathrm{Re}\{\mathrm{k}_{11}^{\mathrm{f}_1}\}B_{L_1} - \mathrm{Re}\{\mathrm{k}_{12}^{\mathrm{f}_1}\}B_{L_2} + \mathrm{Im}\{\mathrm{k}_{15}^{\mathrm{f}_1}\}B_{L_1}B_{L_2} = 0 \tag{27b}$$

$$\mathrm{Re}\{\mathrm{r}_1^{\mathrm{f}_2}\} + \mathrm{Im}\{\mathrm{k}_{13}^{\mathrm{f}_2}\}B_{L_3} + \mathrm{Im}\{\mathrm{k}_{14}^{\mathrm{f}_2}\}B_{L_4} + \mathrm{Re}\{\mathrm{k}_{1(10)}^{\mathrm{f}_2}\}B_{L_3}B_{L_4} = 0 \tag{27c}$$

$$\mathrm{Im}\{\mathrm{r}_1^{\mathrm{f}_2}\} - \mathrm{Re}\{\mathrm{k}_{13}^{\mathrm{f}_2}\}B_{L_3} - \mathrm{Re}\{\mathrm{k}_{14}^{\mathrm{f}_2}\}B_{L_4} + \mathrm{Im}\{\mathrm{k}_{1(10)}^{\mathrm{f}_2}\}B_{L_3}B_{L_4} = 0 \tag{27d}$$

Finally, the analytic results are:

$$B_{L_1} = \frac{\mathrm{Im}\{\mathrm{k}_{11}^{\mathrm{f}_1}(\mathrm{k}_{12}^{\mathrm{f}_1})^*\} + \mathrm{Im}\{\mathrm{r}_1^{\mathrm{f}_1}(\mathrm{k}_{15}^{\mathrm{f}_1})^*\} \pm \sqrt{\mathrm{A}}}{2\,\mathrm{Re}\{\mathrm{k}_{11}^{\mathrm{f}_1}(\mathrm{k}_{15}^{\mathrm{f}_1})^*\}} \tag{28a}$$

$$B_{L_2} = \frac{\mathrm{Im}\{(\mathrm{k}_{11}^{\mathrm{f}_1})^*\mathrm{k}_{12}^{\mathrm{f}_1}\} + \mathrm{Im}\{\mathrm{r}_1^{\mathrm{f}_1}(\mathrm{k}_{15}^{\mathrm{f}_1})^*\} \mp \sqrt{\mathrm{A}}}{2\,\mathrm{Re}\{\mathrm{k}_{12}^{\mathrm{f}_1}(\mathrm{k}_{15}^{\mathrm{f}_1})^*\}} \tag{28b}$$

$$B_{L_3} = \frac{\mathrm{Im}\{\mathrm{k}_{13}^{\mathrm{f}_2}(\mathrm{k}_{14}^{\mathrm{f}_2})^*\} + \mathrm{Im}\{\mathrm{r}_1^{\mathrm{f}_2}(\mathrm{k}_{1(10)}^{\mathrm{f}_2})^*\} \pm \sqrt{\mathrm{B}}}{2\,\mathrm{Re}\{\mathrm{k}_{13}^{\mathrm{f}_2}(\mathrm{k}_{1(10)}^{\mathrm{f}_2})^*\}} \tag{28c}$$

$$B_{L_4} = \frac{\mathrm{Im}\{(\mathrm{k}_{13}^{\mathrm{f}_2})^*\mathrm{k}_{14}^{\mathrm{f}_2}\} + \mathrm{Im}\{\mathrm{r}_1^{\mathrm{f}_2}(\mathrm{k}_{1(10)}^{\mathrm{f}_2})^*\} \mp \sqrt{\mathrm{B}}}{2\,\mathrm{Re}\{\mathrm{k}_{14}^{\mathrm{f}_2}(\mathrm{k}_{1(10)}^{\mathrm{f}_2})^*\}} \tag{28d}$$

with

$$\begin{aligned}\mathrm{A} &= \mathrm{Im}\left\{\mathrm{k}_{11}^{\mathrm{f}_1}(\mathrm{k}_{12}^{\mathrm{f}_1})^*\right\}^2 + \mathrm{Im}\left\{\mathrm{r}_1^{\mathrm{f}_1}(\mathrm{k}_{15}^{\mathrm{f}_1})^*\right\}^2 + 2\,\mathrm{Re}\left\{\mathrm{r}_1^{\mathrm{f}_1}(\mathrm{k}_{11}^{\mathrm{f}_1})^*\right\}\mathrm{Re}\left\{\mathrm{k}_{12}^{\mathrm{f}_1}(\mathrm{k}_{15}^{\mathrm{f}_1})^*\right\} \\ &\quad +2\,\mathrm{Re}\left\{\mathrm{r}_1^{\mathrm{f}_1}(\mathrm{k}_{12}^{\mathrm{f}_1})^*\right\}\mathrm{Re}\left\{\mathrm{k}_{11}^{\mathrm{f}_1}(\mathrm{k}_{15}^{\mathrm{f}_1})^*\right\}, \\ \mathrm{B} &= \mathrm{Im}\left\{\mathrm{k}_{13}^{\mathrm{f}_2}(\mathrm{k}_{14}^{\mathrm{f}_2})^*\right\}^2 + \mathrm{Im}\left\{\mathrm{r}_1^{\mathrm{f}_2}(\mathrm{k}_{1(10)}^{\mathrm{f}_2})^*\right\}^2 + 2\,\mathrm{Re}\left\{\mathrm{r}_1^{\mathrm{f}_2}(\mathrm{k}_{13}^{\mathrm{f}_2})^*\right\}\mathrm{Re}\left\{\mathrm{k}_{14}^{\mathrm{f}_2}(\mathrm{k}_{1(10)}^{\mathrm{f}_2})^*\right\} \\ &\quad +2\,\mathrm{Re}\left\{\mathrm{r}_1^{\mathrm{f}_2}(\mathrm{k}_{14}^{\mathrm{f}_2})^*\right\}\mathrm{Re}\left\{\mathrm{k}_{13}^{\mathrm{f}_2}(\mathrm{k}_{1(10)}^{\mathrm{f}_2})^*\right\}.\end{aligned}$$

As can be seen, if $\mathrm{A} < 0$, then there are no solutions for B_{L_1} and B_{L_2}. The same fact applies to B, B_{L_3}, and B_{L_4}. In Fig. 16 for each case the first solution of the load susceptances over frequency is depicted. In addition, the colored areas are indicating the frequency ranges, with $\mathrm{A} < 0$ and $\mathrm{B} < 0$. Obviously, there are continuous solutions from 0.83 GHz to 1.1 GHz as an exemplary reconfiguration range. For f_1 and f_2 all susceptances have positive sign, meaning all loads are capacitors. In Table 2 the load locations, the theoretical capacitances and the ones that can be found off the shelf are listed. These values are inserted in the simulation to determine the reflection coefficients, which are given in Fig. 17. The dashed curves (blue for f_1 and cyan for f_2) showing the reflection coefficients, when the

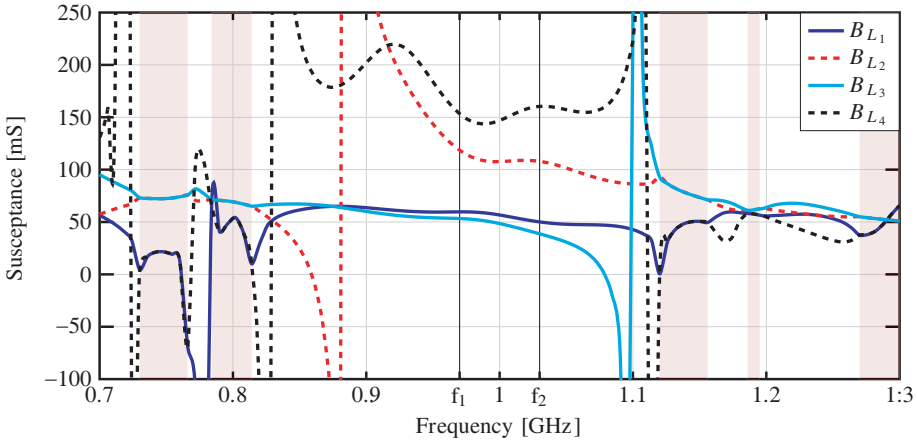

Figure 16. In each case the first solution of the load susceptances over frequency. The coloured areas are indicating the frequency range where, $\mathrm{A} < 0$ and $\mathrm{B} < 0$, therefore, in this range no valid solution is available.

Table 2. The locations, the theoretical and, off the shelf values of the calculated load capacitors.

Cap.	Loc. (x, y) [mm]	Theo. val. [pF]	off the shelf val. [pF]
C_1	$(25, 15)$	9.7926	10
C_2	$(25, 5)$	19.4519	18
C_3	$(25, -5)$	5.9838	5.6
C_4	$(25, -15)$	24.7821	27

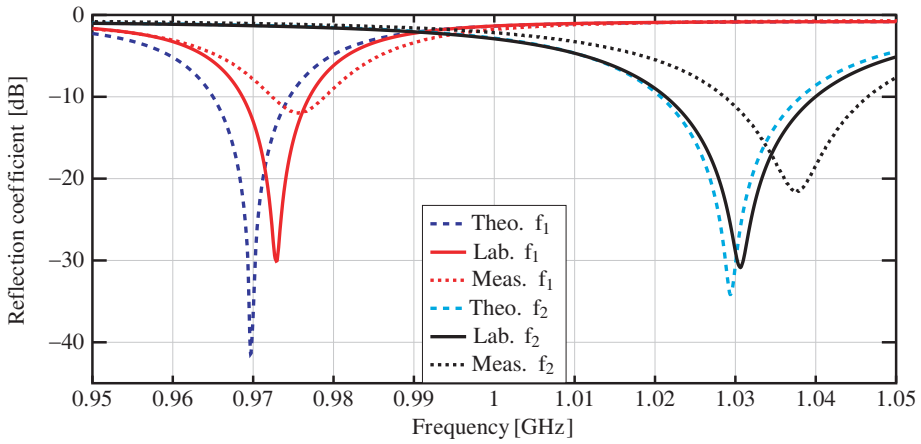

Figure 17. The reflection coefficient over frequency in dB, when the loads, according to Table 2 are inserted.

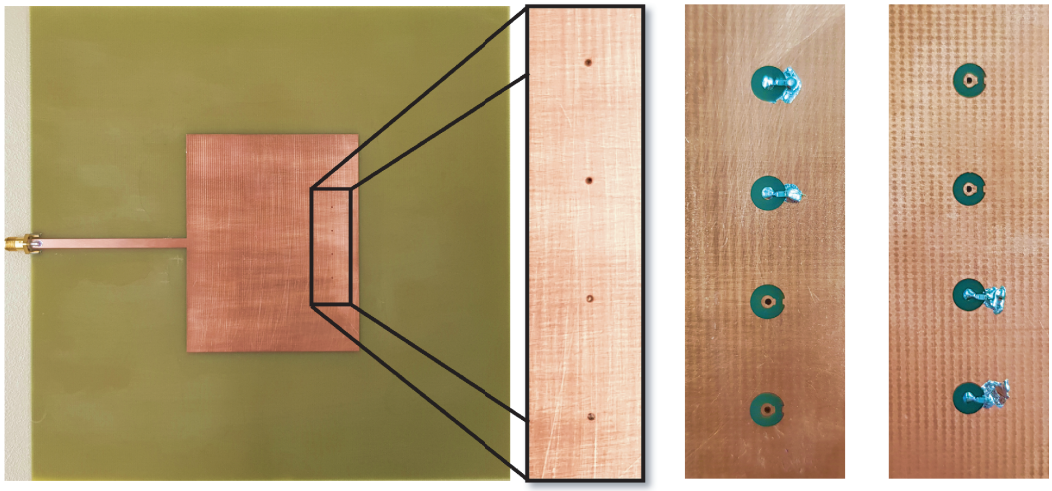

Figure 18. Photograph of the prototype; (a) top view, (b) top view with zoom into the load vias area, (c) the soldered capacitors for "f_1" and (d) the capacitors for "f_2".

theoretical calculated capacitances are applied, while the solid curves showing the ones, when off the shelf values are used.

A prototype is manufactured as can be seen in the photograph of Fig. 18. The values of the load capacitors are chosen according to the available values. In Fig. 18(a) the top view of the whole patch is depicted, while (b) shows a zoom-in view on the load via area. (c) and (d) show the two cases,

f_1 and f_2. To cover both scenarios, two PCB are manufactured, which differ only by load capacitors and their locations. This approximates the switching. The measured reflection coefficient for the cases f_1 and f_2 are shown in Fig. 17. A deviation from the simulation is evident but in an understandable range since the whole structure has very narrow bandwidth. At this point, one critical issue should be mentioned. Namely, the dimensions of the load ports have, understandable, significant impact on the load admittance values. So, when the multi port parameters are determined one should keep in mind to precisely define the port dimensions, especially if it is a narrow-band structure. In this work the edge length of the load ports is set to 0.6 mm, and the capacitors package is 0402, which has a width of about 0.5 mm. The capacitance values have a tolerance of about $\pm 5\%$.

4. CONCLUSION

The main outcome of the theory presented in this paper is a nonlinear equation system. Thereby, the solution variables are the load admittances of a multi port antenna with an arbitrary number of feed and load ports. If this equation system is fulfilled complex conjugate impedance matching at all feed ports at one particular frequency is obtained. It is further shown how this equation system is simplified when some of the loads are switched off. One finding is that two reactive components per feed port are required to realize lossless matching.

To verify the theory, three examples are presented. The first one is a square patch antenna with two feed and four load ports. It has be shown that with the four load components, which are calculated with the theory, both feed ports are losslessly matched. Also, it is shown how the loads change with the location and over frequency. The second example deals with a single-fed rectangular patch antenna with only one load, for which the load impedance distribution over the whole structure is analytically determined. Regions are computed, in which the load is capacitive and for other regions inductive. Further, two curves on the patch are found, on which the real part of the load is zero, meaning that at these locations, lossless matching with only one component is possible. In the third example, a single-fed rectangular patch antenna with four purely reactive, lossless loads is considered. Thereby, two different frequencies should be reconfigurable. Therefore, for each frequency two load components should serve, while the respective other two are excluded. Analytical formulae for the load admittances are given and verified by simulations and by measurements of prototypes.

The proposed technique can be applied to other antenna structures. Further work should include the switching capability: The behavior of these switches at the design frequency can be included as known part of the load admittances.

ACKNOWLEDGMENT

This work was supported in part by the German Research Foundation (DFG) under grant HE6429/7-2. I would also like to thank Dr.-Ing. Ning Yan Zhu for the fruitful discussion related to this work.

REFERENCES

1. Bahl, I., P. Bhartia, and S. Stuchly, "Design of microstrip antennas covered with a dielectric layer," *IEEE Trans. Antennas Propag.*, Vol. 30, No. 2, 314–318, Mar. 1982.
2. Shavit, R., "Dielectric cover effect on rectangular microstrip antenna array," *IEEE Trans. Antennas Propag.*, Vol. 42, No. 8, 1180–1184, Aug. 1994.
3. Rano, D., M. A. Chaudray, and M. S. Hashmi, "New model to determine effective permittivity and resonant frequency of patch antenna covered with multiple dielectric layers," *IEEE Access*, Vol. 8, 34418–34430, 2020.
4. Soares, A., S. Fonseca, and A. Giarola, "The effect of a dielectric cover on the current distribution and input impedance of printed dipoles," *IEEE Trans. Antennas Propag.*, Vol. 32, No. 11, 1149–1153, Nov. 1984.
5. Bailey M. and C. Swift, "Input admittance of a circular waveguide aperture covered by a dielectric slab," *IEEE Trans. Antennas Propag.*, Vol. 16, No. 4, 386–391, Jul. 1968.

6. Bailey, M., "Input admittance of a circular waveguide aperture covered by a dielectric slab," *IEEE Trans. Antennas Propag.*, Vol. 18, No. 5, 596–603, Sep. 1970.
7. Behera, S. K. and N. C. Karmakar, "Wearable chipless radio-frequency identification tags for biomedical applications: A review [antenna applications corner]," *IEEE Antennas and Prop. Mag.*, Vol. 62, No. 3, 94–104, Jun. 2020.
8. Griffin, J. D., G. D. Durgin, A. Haldi, and B. Kippelen, "RF tag antenna performance on various materials using radio link budgets," *IEEE Antennas Wireless Propag. Lett.*, Vol. 5, 247–250, 2006.
9. Ivsic, B., G. Golemac, and D. Bonefacic, "Performance of wearable antenna exposed to adverse environmental conditions," *ICECom 2013*, 1–4, 2013.
10. Lilja, J., P. Salonen, T. Kaija, and P. de Maagt, "Design and manufacturing of robust textile antennas for harsh environments," *IEEE Trans. Antennas Propag.*, Vol. 60, No. 9, 4130–4140, Sep. 2012.
11. Smith, G., "Directive properties of antennas for transmission into a material half-space," *IEEE Trans. Antennas Propag.*, Vol. 32, No. 3, 232–246, Mar. 1984.
12. Warren, C., N. Chiwaridzo, and A. Giannopoulos, "Radiation characteristics of a high-frequency antenna in different dielectric environments," *Proc. of the 15th Int. Conf. on Ground Penetrating Radar*, 767–772, 2014.
13. Foster, P. R., "Antenna problems in RFID systems," *IEE Colloquium on RFID Technol. (Ref. No. 1999/123)*, 3/1–3/5, 1999.
14. Dobkin, D. and S. Weigand, "Environmental effects on RFID tag antennas," *IEEE MTT-S Int. Microw. Symp. Dig., 2005*, 135–138, 2005.
15. Karthika, K. and K. Kavitha, "Reconfigurable antennas for advanced wireless communications: A review," *Wireless Pers. Commun.*, Vol. 120, No. 4, 2711–2771, May 2021.
16. Srivastava, M. and A. Kumar, "A review paper on reconfigurable antenna technique and methodology," *Emerging Technologies in Data Mining and Information Security. Lecture Notes in Networks and Systems*, J. M. R. S. Tavares, S. Chakrabarti, A. Bhattacharya, and S. Ghatak (eds.), Vol. 164, 605–615, Singapore, Springer, 2021.
17. Christodoulou, C. G., Y. Tawk, S. A. Lane, and S. R. Erwin, "Reconfigurable antennas for wireless and space applications," *Proc. of the IEEE*, Vol. 100, No. 7, 2250–2261, Jul. 2012.
18. Costantine, J., Y. Tawk, S. E. Barbin, and C. G. Christodoulou, "Reconfigurable antennas: Design and applications," *Proc. of the IEEE*, Vol. 103, No. 3, 424–437, Mar. 2015.
19. Oliveri, G., D. H. Werner, and A. Massa, "Reconfigurable antennas: Design and applicationsreconfigurable electromagnetics through metamaterials — A review," *Proc. of the IEEE*, Vol. 103, No. 7, 1034–1056, Jul. 2015.
20. Haupt, R. L. and M. Lanagan, "Reconfigurable antennas," *IEEE Antennas and Prop. Mag.*, Vol. 55, No. 1, 49–61, Feb. 2013.
21. Pringle, L. N., P. H. Harms, S. P. Blalock, G. N. Kiesel, E. J. Kuster, P. G. Friederich, R. J. Prado, J. M. Morris, and G. S. Smith, "A reconfigurable aperture antenna based on switched links between electrically small metallic patches," *IEEE Trans. Antennas Propag.*, Vol. 52, No. 6, 1434–1445, Jun. 2004.
22. Soltani, S., P. Lotfi, and R. D. Murch, "Design and optimization of multiport pixel antennas," *IEEE Trans. Antennas Propag.*, Vol. 66, No. 4, 2049–2054, Apr. 2018.
23. Lotfi, P., S. Soltani, and R. D. Murch, "Printed endfire beam-steerable pixel antenna," *IEEE Trans. Antennas Propag.*, Vol. 65, No. 8, 3913–3923, Aug. 2017.
24. Jiang, F., C.-Y. Chiu, S. Shen, Q. S. Cheng, and R. Murch, "Pixel antenna optimization using N-port characteristic mode analysis," *IEEE Trans. Antennas Propag.*, Vol. 68, No. 5, 3336–3347, May 2020.
25. Jiang, F., S. Shen, C.-Y. Chiu, Z. Zhang, Y. Zhang, Q. S. Cheng, and R. Murch, "Pixel antenna optimization based on perturbation sensitivity analysis," *IEEE Trans. Antennas Propag.*, Vol. 70, No. 1, 472–486, Jan. 2022.

26. Quijano, J. L. A. and G. Vecchi, "Optimization of an innovative type of compact frequency-reconfigurable antenna," *IEEE Trans. Antennas Propag.*, Vol. 57, No. 1, 9–18, Jan. 2009.
27. Ogawa, K., T. Takahashi, Y. Koyanagi, and K. Ito, "Automatic impedance matching of an active helical antenna near a human operator," *33rd Eur. Microw. Conf. Proc. (IEEE Cat. No.03EX723C)*, Vol. 3, 1271–1274, 2003.
28. deMingo, J., A. Valdovinos, A. Crespo, D. Navarro, and P. Garcia, "An RF electronically controlled impedance tuning network design and its application to an antenna input impedance automatic matching system," *IEEE Trans. Microw. Theory Techn.*, Vol. 52, No. 2, 489–497, Feb. 2004.
29. Huang, L., "Theoretical and experimental investigation of adaptive antenna impedance matching for multiband mobile phone applications," *IEE Wideband and Multi-band Antennas and Arrays 2005 (Ref. No. 2005/11059)*, 13–17, 2005.
30. Qiao, D., Y. Zhao, T. Hung, D. Kimball, M. Li, P. Asbeck, D. Choi, D. Kelly, D. Qiao, et al., "Antenna impedance mismatch measurement and correction for adaptive CDMA transceivers," *IEEE MTT-S Int. Microw. Symp. Dig., 2005*, 783–786, 2005.
31. Hur, B., W. R. Eisenstadt, and K. L. Melde, "Testing and validation of adaptive impedance matching system for broadband antenna," *Electronics*, Vol. 8, No. 9, 1055, Sep. 2019.
32. Liu, F.-X., Z. Xu, D. C. Ranasinghe, and C. Fumeaux, "Textile folded half-mode substrate-integrated cavity antenna," *IEEE Antennas Wireless Propag. Lett.*, Vol. 15, 1693–1697, 2016.
33. Dissanayake, T., K. P. Esselle, and M. R. Yuce, "Dielectric loaded impedance matching for wideband implanted antennas," *IEEE Trans. Microw. Theory Techn.*, Vol. 57, No. 10, 2480–2487, Oct. 2009.
34. Soontornpipit, P., C. M. Furse, and Y. C. Chung, "Design of implantable microstrip antenna for communication with medical implants," *IEEE Trans. Microw. Theory Techn.*, Vol. 52, No. 8, 1944–1951, Aug. 2004.
35. Deleruyelle, T., P. Pannier, M. Egels, and E. Bergeret, "An RFID tag antenna tolerant to mounting on materials," *IEEE Antennas and Prop. Mag.*, Vol. 52, No. 4, 14–19, Aug. 2010.
36. Luomaniemi, R., P. Yla-Oijala, A. Lehtovuori, and V. Viikari, "Designing hand-immune handset antennas with adaptive excitation and characteristic modes," *IEEE Trans. Antennas Propag.*, Vol. 69, No. 7, 3829–3839, Jul. 2021.
37. Fischer, S. B. and J. Hesselbarth, "Power divider network for dual-fed adaptive antenna", *Int. J. of Microw. and Wireless Technol.*, 1–8, Mar. 2022.
38. Jeeninga, M., A. J. van der Schaft, and C. De Persis, "Graph theoretic formulae for the determinant and adjugate of Matrices carrying Graph Structure," *IFAC-Papers OnLine*, Vol. 51, No. 23, 259–264, 2018.